New Journal of Physics
The open access journal at the forefront of physics

Deutsche Physikalische Gesellschaft DPG IOP Institute of Physics

Thermal contact delocalization in atomic scale friction: a multitude of friction regimes

To cite this article: Sergey Yu Krylov and Joost W M Frenken 2007 *New J. Phys.* **9** 398

New Journal of Physics
The open-access journal for physics

Thermal contact delocalization in atomic scale friction: a multitude of friction regimes

Sergey Yu Krylov[1,2,3] **and Joost W M Frenken**[1]

[1] Kamerlingh Onnes Laboratory, Leiden University, 2300 RA Leiden, The Netherlands
[2] Institute of Physical Chemistry, Russian Academy of Sciences, 119991 Moscow, Russia
E-mail: krylov@redline.ru and frenken@physics.leidenuniv.nl

New Journal of Physics **9** (2007) 398
Received 16 July 2007
Published 31 October 2007
Online at http://www.njp.org/
doi:10.1088/1367-2630/9/10/398

Abstract. This paper summarizes and extends results from a series of recent investigations of atomic scale friction, in which an ultra-low effective mass and a corresponding thermal delocalization of the contact play a dominant role. A rich variety of physically different regimes of friction concerned with the contact delocalization are analyzed in a systematic way and visualized by advanced numerical calculations. The results shed an essentially new light on what is actually measured in friction force microscopy and suggest the necessity to reinterpret many seemingly standard experiments. Even more importantly, our results can possibly be extended to the asperities that establish the contact between two sliding bodies thus predicting a much more pronounced role of thermally driven dynamics in macroscopic sliding than has ever been imagined. The paper is supplied with a detailed introduction to the subject, aimed at a general physical audience.

[3] Author to whom any correspondence should be addressed.

PII: S1367-2630(07)55255-9

Contents

1. Introduction

From the point of view of a physicist, even of one specializing in surface science, friction may seem a relatively simple phenomenon. The friction laws one is taught at university were formulated as early as the 18th century, by Amontons and Coulomb, and they had even been found much earlier by Leonardo da Vinci [1]. Friction is concerned with dissipation of momentum. Clearly, one can imagine various microscopic mechanisms for this dissipation, depending on the temporal and spatial scales involved. The details are apparently complex/cumbersome and may seem to form an issue only in an engineering context, rather than to establish a fundamental challenge. Actually, this is not so. As mentioned by R P Feynman in 1963, 'It is quite difficult to do quantitative experiments in friction, and the laws of friction are still not analyzed very well, in spite of the enormous engineering value . . . At the present time, in fact, it is impossible even to estimate the coefficient of friction between two substances' [2]. Up to now, one has not come too far beyond this poor level of understanding, in spite of the

intense investigations performed during the last three decades within the newborn and rapidly developing science of tribology [3]–[5]. Friction appears to become even more of a puzzle than one could think, and both the microscopic mechanisms of dissipation and their manifestation in sliding between macroscopic bodies remain shrouded in mystery.

1.1. Atomic force microscope (AFM)/friction force microscope (FFM)

Shortly after the invention of the AFM this instrument was also applied [6] as a FFM. In FFM experiments an atomically sharp tip is dragged along a surface by an external spring (the cantilever), similar to AFM, and the lateral force is recorded with nanonewton (nN) or even piconewton (pN) sensitivity. This seemingly trivial extension of the AFM to the lateral direction has enjoyed great interest [4]. The FFM tip is believed to model the behavior of a single asperity, similar to one of the many asperities that make up the contact between two macroscopic sliding bodies, and thus provide direct, atomic scale access to the origin of friction. Experiments with atomic resolution typically, though not universally, demonstrate a periodic, sawtooth-like behavior of the lateral force, with the period of the substrate lattice. This phenomenon is known as atomic stick-slip (SS) [4]. The FFM tip is thought to be held periodically in a substrate lattice position until the increasing external force becomes sufficient to force the tip to slip to the neighboring lattice position, after which the cycle repeats itself.

1.2. Prandtl–Tomlinson model

Atomic SS is easily modeled using a simple approach, first proposed by Prandtl [7] and often referred to as the Tomlinson model [8]. An object (the tip) is considered to move in a periodic potential field formed by its interaction with the substrate lattice. It is dragged along the surface by a rigid, external support, via a macroscopic spring (the cantilever), which is at the same time used to measure the lateral force experienced. The total potential energy of the system, which consists of the sum of the periodic, to first approximation sinusoidal tip–surface interaction and the parabolic contribution of the deformed spring, contains a number of wells which periodically appear, change and disappear in the cause of scanning. Within the Prandtl–Tomlinson model, the tip is assumed to reside in a certain well until this well ceases to exist. This is the ‘stick’ part of the motion cycle. At a certain, critical position of the support the well in which the system resides vanishes. This can be viewed as a mechanical instability and the tip slips to the neighboring well. Implicitly, in this model the dissipation of energy is assumed to take place very efficiently during the slip events, when the tip moves rapidly with respect to the surface.

Per lattice spacing, the lateral force goes through significant variations that may even involve changes in sign, from reverse to forward forces. The friction force is the average value of the lateral force and corresponds to the average amount of energy dissipated per unit traveled distance.

Several at first glance surprising but actually very general results are predicted by the Prandtl–Tomlinson model already in the simplest, quasistatic approximation, when one assumes complete dissipation of the excess energy in each slip event. First, the friction force is independent of the microscopic dissipation rate. This means that the relation between friction and dissipation is generally far from direct. A second, related surprise is that friction depends not only on the corrugation of the interaction potential between the surfaces in contact, but equally strongly on the stiffness of the driving spring. This instructive observation manifests the

fact that the overall energy loss should depend on both how energy is dissipated by the system and how effectively it is invested.

The third remarkable result of the Prandtl–Tomlinson model is the prediction of a transition from SS to continuous, near-frictionless sliding, the regime is often called superlubricity (SL) [9]. This transition takes place at a critical value of the relative potential corrugation, with respect to the stiffness of the driving spring. Below this corrugation, the total potential has only one well at any position of the support. In other words, the tip always resides in a continuously moving energy optimum and mechanical instabilities do not occur. Interestingly, this SL can occur even at very high amplitudes of the interaction potential, provided the spring is hard enough. The transition from SS to continuous, low-dissipative sliding has been observed in recent experiments [10, 11]. One of the aims of the present paper is to show that the physics behind this transition is richer and the transition criteria can be different from earlier, naive expectations.

In its simplest, quasistatic form the Prandtl–Tomlinson model predicts velocity- and temperature-independent friction. Even though this can be a reasonable approximation for certain conditions, it fails in a broader context. General physical arguments can be used to show that one should expect a linear dependence of friction on velocity in the two limiting cases of low and high velocities. The role of temperature is even less clear in advance. Generalizations of the Prandtl–Tomlinson model, from dynamical modeling to nonequilibrium statistical mechanics [12], have advanced our understanding of atomic scale friction, e.g. its velocity dependence, possible transitions from SS to other regimes and the role of thermal effects [13]–[16]. Here, we will mainly concentrate on thermal effects. As will be shown below, this aspect of the problem turns out to be much more important in atomic friction than imagined thus far.

1.3. Is temperature important?

The possible role of temperature in friction was anticipated as early as 1928 by Prandtl [7], but experimental and theoretical evidence has appeared only recently. As was shown experimentally and theoretically in a series of studies by E Meyer and co-workers at Basel University [13, 17, 18] and also in calculations by other groups [14, 19, 20], thermal activation can play an important role in the motion of the tip along the surface. Before the position of mechanical instability is reached, the tip experiences a lateral potential barrier to the next well, the height of which decreases as the instability is approached and becomes equal to zero at the critical point. Consequently, at nonzero temperature, the tip will always perform a thermally activated jump over this decreasing barrier, thus slipping to the next well somewhat earlier than expected on the basis of purely mechanistic arguments. These activated, pre-critical jumps of the FFM tip manifest themselves in statistical variations in both the positions of slip events and the amplitude of the lateral force, as typically observed in experiments. Furthermore, they are at the origin of a weak, logarithmic or logarithmic-like velocity dependence of friction in the SS regime, as first observed in [13].

1.4. Thermolubricity (TL)

One can extend the idea of thermal activation of the tip motion to the seemingly extreme case of multiple jumps of the tip back and forth between the available potential wells. This

scenario necessarily becomes manifest at sufficiently low velocities or high temperatures or for sufficiently low corrugations of the potential. As we have shown before [16], such multiple jumps can be important at quite typical experimental conditions, leading to a substantial suppression of friction in a range of relatively low but supercritical potential energy corrugations. We have introduced the term thermolubricity (TL) to denote this thermally-induced slipperiness. Our analytical and numerical calculations, performed within a generalized one-spring Prandtl–Tomlinson model combined with a rate theory description of the thermal motion of the tip, have produced excellent agreement with experiments [16], thus suggesting a very pronounced role of thermally activated jumps, indeed. Interestingly, these observations have generated a new collection of questions. For example, one of the crucial parameters in the TL model is the pre-exponential factor for the thermally excited jumps. This factor may be viewed as the attempt frequency for these thermal jumps. The value of this pre-exponential factor obtained from comparison with experiments turned out to be comparable with the mechanical eigenfrequency of the cantilever for one particular experimental system with a soft cantilever [10]. However, a much smaller pre-exponential factor was found for another system with a more conventional, hard cantilever [11]. Although arguments can be formulated to explain both of these results separately, it is not easy to explain the order of magnitude difference between the prefactors in these experiments. Another question of a more general nature is how thermal activation, a phenomenon natural for atomically small objects (e.g. in surface diffusion of atoms [21, 22] and even large atomic clusters [23, 24]), can play such an essential role in the motion of a massive, macroscopic object such as the entire cantilever. Here, we are confronted with the failure of the traditional one-mass-one-spring approach to atomic friction, as we will demonstrate below.

1.5. Tip flexibility and effective mass of the contact

A basic issue, which has not been fully recognized yet, is concerned with flexibility of the FFM tip. At first glance, the typical silicon, silicon nitride or metal tips seem very hard objects. However, the spring constant, measured in experiments from the restoring forces at small, sub-atomic support displacements, is usually much smaller than the stiffness K of the cantilever. It can be presented as $k_{\mathrm{eff}} = (K^{-1} + k^{-1})^{-1}$, with k_{eff}, and hence k, typically of the order of $1\,\mathrm{N\,m^{-1}}$, i.e. of the order of the stiffness of atomic bonds. There is no other way than to associate k with the flexibility of the tip, which hence turns out to be even softer than most cantilevers, irrespective of the material and precise shape of the tip [10, 11, 13, 25]. This inherent feature has long been believed not to complicate the SS physics. Traditionally, FFM is therefore described by a single-spring Prandtl–Tomlinson model, in which an effective mass, close to that of the cantilever, is dragged along the surface by an effective spring k_{eff}, which accounts for the flexibility of both the cantilever and the tip. First experimental and theoretical indications for the failure of the one-spring approach have appeared only recently [15], [26]–[30]. Flexibility of the tip introduces an additional channel of dissipation into the system that can lead to a nonmonotonous velocity dependence of friction [15, 31]. Another manifestation of the tip flexibility, as concluded from simulations of a two-spring system [26], is in the duration of slip events.

For a true understanding of the dynamics, we must explore at least a two-mass-two-spring scheme (see figure 1), with one real mass (M) accounting for the combined cantilever+tip inertia, and the other—effective mass (m) associated with the bending motion of the tip.

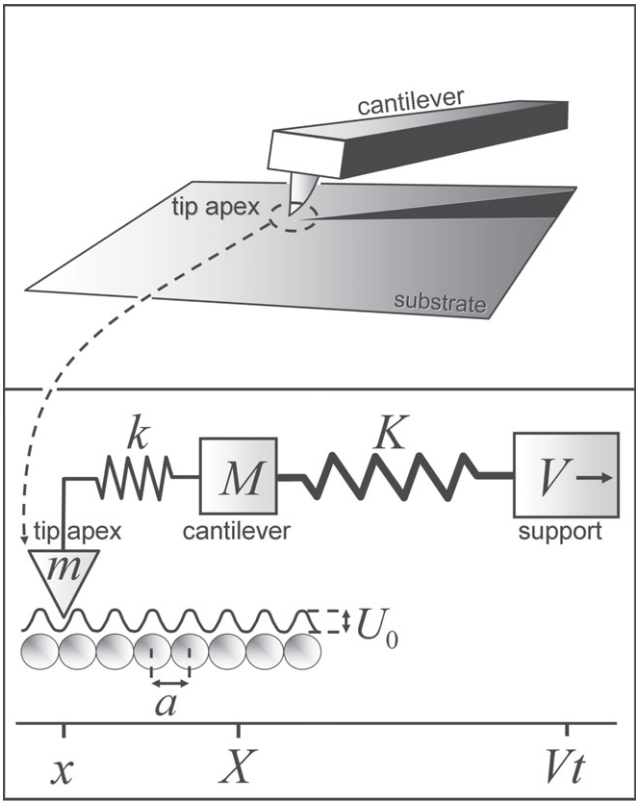

Figure 1. Schematic of the measuring system in FFM and the corresponding two-mass-two-spring model geometry analyzed in this paper. K is the spring coefficient of the cantilever and k is the spring coefficient associated with the tip apex. M is the mass of the cantilever+tip system and m is an effective mass, representing the tip apex. The apex interacts with the substrate, which is modeled by a sinusoidal potential with a corrugation U_0 and with the period a of the substrate lattice. The system is driven by a rigid support that moves with a constant velocity V. The positions of the support, the cantilever and the tip apex are denoted by Vt, X and x, respectively, where the situation of undistorted springs corresponds to $x = X = Vt$.

Generally, this can introduce a wealth of new dynamics. The key question is how small the characteristic value is of the effective mass m.

According to our calculations [28], the bending deformation of an atomically sharp conical or pyramidal tip is associated with only a few hundred atomic layers at its apex, so that the effective mass $m \sim 10^{-20}$ kg, while the typical mass M of the tip–cantilever combination is 9–12 orders of magnitude higher. If we combine the small effective mass with the spring coefficient k of the tip apex, we find that the characteristic frequency of the tip apex bending vibration (ν_t) should be in the order of several GHz, while the characteristic cantilever frequencies (ν_c) fall in the kHz to MHz range. A very strong hierarchy between the effective masses and the effective frequencies involved in the problem can lead to at least two important, potentially dramatic consequences. Firstly, the low-frequency response of the system as measured in FFM experiments from the motion of the cantilever can be very different from the rapid motion

that is actually performed by the ultra-low effective mass, which is really probing the surface. Secondly, the role of thermal effects in the tip–surface coupling can be much stronger than one could ever expect for a system with a single mass or a two-mass system with similar frequencies.

1.6. 'Stuck in slipperiness' (SinS)

On the basis of analytical and numerical calculations in the framework of a simplified statistical–mechanical description of a two-mass-two-spring system, with one of the masses ultra-low, as argued above, we have predicted [28] a new, strongly counterintuitive regime of friction to be characteristic (observable) for systems with sufficiently soft cantilevers at moderate corrugations of the tip–surface interaction potential. The cantilever shows seemingly usual atomic SS, while the tip–surface contact is completely delocalized due to rapid, thermally activated motion of the tip apex back and forth between the available potential wells. In this SinS regime friction is low but not zero.

The interesting physics encountered here can be understood in the following way. If the rate r of thermally activated tip apex jumps between neighboring potential wells strongly exceeds the characteristic frequency ν_c of the cantilever, which is a situation typical for $m \lll M$, the cantilever cannot follow the rapid thermal motion of the contact. Instead, it experiences the effective surface interaction that remains after averaging over this rapid motion. This effective potential is corrugated and still exhibits the period of the substrate lattice. If the cantilever is sufficiently soft, it experiences SS motion in this effective potential, precisely in the manner predicted by the usual one-spring Prandtl–Tomlinson model.

Importantly, both the amplitude and the shape of the effective potential are essentially different with respect to the true interaction between the tip apex and the surface (see figure 3 in [28]). As a consequence, the relation between FFM observables, such as the amplitude of the recorded lateral force on the cantilever, and physical parameters of the system, such as the corrugation of the interaction potential, become quite different with respect to the predictions of the traditional, one-effective-spring Prandtl–Tomlinson model.

At high amplitudes of the potential, when $r \ll \nu_c$, the thermally activated motion of the tip apex plays a minor role, and the system exhibits ordinary SS. At intermediate corrugations, when $r \gtrsim \nu_c$, one can expect stochastic behavior of the system, which requires a separate, typically numerical analysis.

1.7. Evidence for contact delocalization

Unfortunately, a full Langevin description of the two-mass-two-spring system, as used in [26], is not realistic for $m \lll M$ for computational reasons, simply because the characteristic timescales for the two parts of the system are too different, making the calculation time prohibitively long or the precision prohibitively poor. Recently, we have developed a hybrid computational scheme that combines a numerical Langevin description of the cantilever motion with a Monte-Carlo treatment of the thermally activated motion of the tip's apex, the rest of the tip being considered an integral part of the cantilever. The numerical algorithm enables one to completely follow the dynamic interplay between the rapid motion of m and the slow motion of M [32]. The computational scheme is described in detail in the next section.

In a first analysis, we have observed that the slipping of the cantilever—the processes when energy stored in the system is rapidly dissipating—can proceed in several different

ways, depending sensitively on the corrugation of the potential. Besides the 'fast' slipping, there are several characteristic types of slip events that take more time and have nontrivial 'fine structure'. The most remarkable is the slipping via an intermediate state, which looks as if there were an intermediate lattice position, midway between two regular lattice sites. These unusual slips directly reflect delocalization of the tip–surface contact. Our results find remarkably good confirmation in the recent observations by Maier *et al* [26], who performed the first high-resolution experiment in which durations of slip events have been resolved. Our two-mass-two-spring behavior provides a straightforward explanation for these unique experimental findings, which were ascribed by Maier *et al* to a possible but highly improbable configuration of simultaneous contact via several 'nanotips', positioned in a geometry commensurate with the substrate lattice. The excellent agreement of the two-mass-two-spring model with the experiment of [26] is a strong evidence for at least partial delocalization of the tip–surface contact [32]. From simulations for different values of m and comparison with the experiment we find that the actual effective mass of the contact must be very small indeed. Our upper estimate of $m < 10^{-18}$ kg contrasts earlier expectations [26, 31] and supports our recent geometrical estimates [28].

1.8. Aims of this work

As described in the above introduction, an ultra-low effective mass and the related thermal delocalization of the contact in atomic scale friction have been anticipated theoretically and have found experimental confirmation. Our calculations show that the dynamic behavior of the two-mass-two-spring system depends sensitively on the spring constants, the amplitude of the interaction potential and other parameters involved. The rapid transition dynamics of m is *not* washed out in the slow response of M, but leads to the existence of a surprisingly rich variety of different observable regimes, including situations with a delocalized tip–surface contact. Two specific regimes have been discussed by us before [28, 32].

In this paper, we present our analysis of the (presumably) full variety of different physical regimes of friction found within the two-mass-two-spring model with the ultra-low effective mass of the contact. In order to proceed in a systematic way, we will classify the regimes by use of several governing, dimensionless system parameters. These allow us to discuss the physics of the friction regimes, which we visualize with the use of numerical calculations. Several surprising observations are made this way, which could hardly have been anticipated. We will compare two characteristic types of measuring systems, corresponding to either a hard or a soft external spring.

The two-mass-two-spring model unavoidably leads to the conclusion that it is necessary to seriously reinterpret seemingly standard FFM measurements. Although a detailed comparison with experiments is lacking at this stage, we will also briefly touch upon this issue.

2. Theoretical approach

We start with a brief discussion of how a hybrid numerical description of a two-mass-two-spring system is constructed that combines a numerical solution of the Langevin equation for the full cantilever motion with a Monte-Carlo simulation of the thermally activated motion of the tip's apex. This enables one to follow, nearly completely, the dynamic interplay between the rapid motion of m and the slow motion of M.

For a one-dimensional (1D) geometry, the total potential energy of the system (see figure 1) can be written as

$$U(X, x, t) = \frac{K}{2}(Vt - X)^2 + \frac{k}{2}(X - x)^2 + U_s(x), \tag{1}$$

with X and x the coordinates of the cantilever and the tip apex, respectively; Vt is the position of the support that moves with the scanning velocity V; as introduced already, K and k denote the stiffness of the cantilever and of the tip. The tip–surface interaction is assumed to be sinusoidal, with corrugation U_0 and period a, $U_s = \frac{U_o}{2}[1 - \cos(\frac{2\pi x}{a})]$. The system is described by two coupled equations of motion, one for the cantilever+tip combination (position X and mass M) and the other for the tip apex (position x and effective mass m) moving with respect to X. If $m \lll M$, and hence there is a strong hierarchy between the characteristic frequencies of the tip apex (ν_t) and the cantilever (ν_c), $\nu_t \gg \nu_c$, the description can be simplified, without loss of generality, by averaging over the rapid thermal motion of the apex around 'lattice positions' x_i. For each position of the cantilever X, the $x_i(X)$ correspond to the local minima in the total potential (1) as a function of x. The number of wells available to the apex is determined by the Tomlinson-like parameter [28]

$$\gamma = \frac{2\pi^2 U_0}{ka^2}. \tag{2}$$

If $\gamma > 1$, there are two or more wells. Not only is this the origin of SS motion, this also introduces the possibility of thermally activated jumps of the tip apex between the wells. Here, we restrict ourselves to the simplest (transition state theory) approximation to the jump rate:

$$r_{ij} = r_0 \exp\left(-\frac{U_{ij}}{k_B T}\right), \tag{3}$$

with the prefactor $r_0 = \nu_t$, and with $U_{ij}(X)$ the potential barrier between wells i and j. Following this scheme, one can describe the motion of the cantilever by solving numerically only a single Langevin-type equation,

$$M\ddot{X} = -k\,[X - x_i(X)] - K(X - Vt) - M\eta\dot{X} + \xi, \tag{4}$$

in combination with a Monte-Carlo algorithm for transitions of the tip apex between positions x_i and x_j with rate r_{ij}. The random force ξ is normalized as $\langle \xi(t)\xi(t')\rangle = 2M\eta_n k_B T\delta(t - t')$. According to the fluctuation–dissipation theorem for a particle interacting with a bath, $\eta_n = \eta$. In our case, the cantilever is coupled to the bath very indirectly, via motion of the tip apex with respect to the cantilever and with respect to the surface (damping in the cantilever can be neglected [26]). In order to control the possible role of damping and noise, we varied both η and η_n in our calculations. The results presented below correspond to the case of slightly overdamped motion, $\eta = 5\nu_c$, while the noise has been artificially reduced or switched off completely by taking a certain value of $\eta_n < \eta$, in order to better visualize the inherent dynamics of the system. We checked that in a wide range $0.1\,\nu_c < \eta < 10\,\nu_c$ the results do not change qualitatively although they contain stronger fluctuations at lower damping and higher random force amplitude.

An important and new element of this work is that we can follow the behavior of the cantilever, which is the 'observable' in FFM experiments, while seeing simultaneously how the tip apex is actually probing the surface. Several surprises are encountered in this way. In the following three sections, we explore the consequences of the two-mass-two-spring configuration. We start in section 3 by confronting the reader with a counterintuitive example of

the cantilever and apex dynamics. In section 4, we introduce several dimensionless parameters in addition to the one introduced in equation (2). These are used to characterize and classify a variety of regimes of dynamic behavior. After briefly listing these regimes, we illustrate them in more detail in section 5 by use of two series of calculations, one for a soft cantilever and the other for a hard cantilever.

3. Order from chaos

Two examples of calculations with the two-mass-two-spring model are compared in figure 2, for a set of parameters as specified in the caption, typical for a soft and heavy cantilever, such as used in the Leiden FFM [10, 25]. At high amplitude of the interaction potential the cantilever exhibits traditional SS motion (figure 2(A)). It is seen to directly follow the SS motion of the apex (figure 2(B)), very similar to what would be expected within the context of the traditional one-spring model. However, as we will see below, each slip actually goes in two steps. First, the apex slips, on a timescale of ν_t^{-1}, then the entire cantilever follows, on a time scale of ν_c^{-1}. Note that the cantilever motion displays irregularities both in the positions of the slip events and in the maximal values of the lateral force (figure 2(A)) . These reflect the thermal activation of the transition of the apex to the next well prior to the mechanical instability ('pre-critical jump').

At lower corrugation the cantilever also exhibits seemingly usual SS motion (figure 2(C)). However, the tip apex is seen to be completely distributed (delocalized) over two available potential wells, nearly in the full range of support positions (figure 2(D)), due to a very rapid thermally activated motion between the accessible surface wells. This is a direct visualization, in the computer experiment, of the 'SinS' regime predicted in [28]. Due to the finite time resolution in the graph, the displayed number of apex jumps in figure 2(D) is somewhat lower than the actually calculated number of jumps, i.e. the apex is even more delocalized than one can judge from the figure.

Perhaps unexpected, in view of the extremely chaotic motion of the tip apex, is the very regular character of the SS pattern seen in the cantilever response in figure 2(C), which should be compared with the much more irregular pattern in figure 2(A). Against intuition, one sees that chaos leads to order.

The explanation can be found in the comparison of figures 2(B) and (D). If only one (if any) activated jump occurs per lattice spacing traveled, there is a natural statistical variation in the cantilever positions at which the jumps take place (figure 2(B)). If, on the other hand, the jumps are very frequent, the cantilever cannot respond to each of them, but rather follows the average behavior of the apex, which is necessarily regular, simply reflecting the periodicity of the substrate (figure 2(D)). The cantilever moves in the periodic, effective potential obtained by averaging the tip–surface interaction potential over the rapid thermal motion of the apex. This leads to SS motion of the cantilever, provided the amplitude of this effective potential is still high enough and/or the cantilever is soft enough, as is the case in the present example of figures 2(C) and (D). This regular SS pattern is not significantly affected by direct thermal activation of the cantilever itself, due to its huge mass and, hence, low 'attempt' frequency.

If the frequency of thermally activated jumps of the tip apex is intermediate, i.e. neither low nor high, one expects to encounter different types of stochastic behavior of the system, depending sensitively on the values of the parameters involved. This interesting regime will be discussed below in more detail.

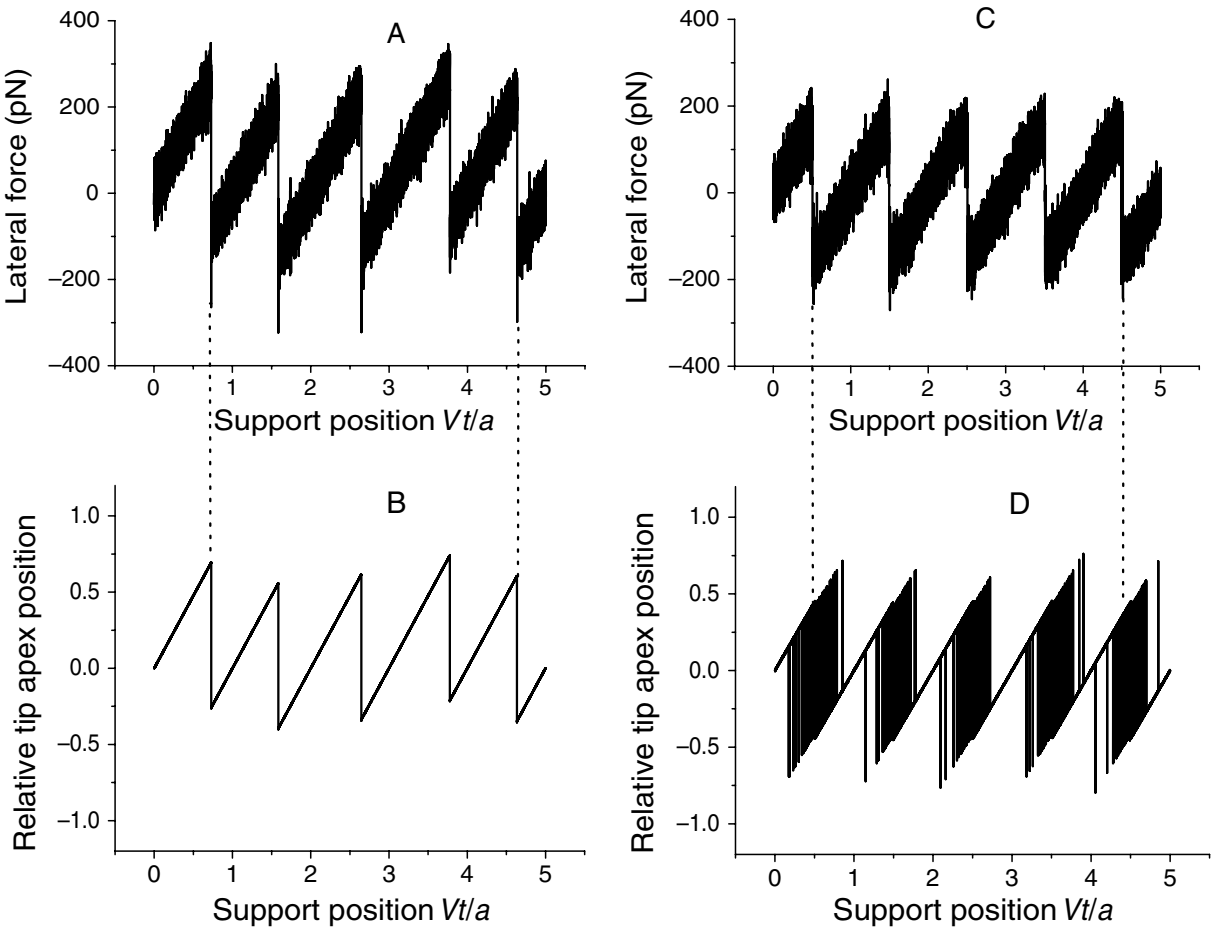

Figure 2. Comparison of calculations of two seemingly similar, traditional cases of SS behavior, (A, B) and (C, D). The two top panels show the lateral forces $F = K(Vt - X)$, recorded on the cantilever and the lower two panels show the position of the tip apex relative to the support, normalized to the lattice period, $(Vt - x)/a$. Thermal noise on the cantilever motion has been artificially reduced by a factor of 5 ($\eta/\nu_c = 5$, $\eta_n/\nu_c = 0.2$) in order to better visualize the inherent dynamics of the system. The left two panels are for a corrugation of the interaction potential of $U_0 = 0.6\,\text{eV}$ and the two panels on the right are for $U_0 = 0.25\,\text{eV}$. The other parameters have been chosen equal in both calculations: temperature $T = 300\,\text{K}$, scanning velocity $V = 3\,\text{nm}\,\text{s}^{-1}$, cantilever stiffness $K = 6\,\text{N}\,\text{m}^{-1}$, tip stiffness $k = 2\,\text{N}\,\text{m}^{-1}$, cantilever mass $M = 1 \times 10^{-9}\,\text{kg}$, effective mass of the tip apex $m = 10^{-21}\,\text{kg}$, and surface lattice spacing $a = 0.25\,\text{nm}$. While the lateral forces in (A) reflect true SS behavior of the contact (B), the seemingly similar force variations in (C) are the result of highly dynamic behavior of the nearly completely delocalized tip apex (D). Note, that the time resolution in the plotted tip apex positions in panel (D) is too coarse to display all calculated jumps.

4. Parameters and regimes

In order to analyze systematically the possible, physically different regimes of friction, we first introduce the relevant, governing parameters of the system.

4.1. Parameters

The two-mass-two-spring model is fully characterized by the following quantities: the corrugation (U_0) and period (a) of the tip–surface interaction potential, the stiffness of the cantilever (K) and that of the tip apex (k), the mass of the cantilever (in a strict sense, this should be the mass of the cantilever+tip combination) (M) and the effective mass of the tip apex (m), the temperature (T), and the scanning velocity (V). Furthermore, in a complete Langevin description there would be three damping parameters in the model: damping of the cantilever motion with respect to the surface (η), damping of the tip apex motion with respect to the surface (η_{ts}) and damping of the tip apex motion with respect to the cantilever, i.e. of the bending motion of the tip (η_{t}). In the rate description of the tip apex motion, instead of η_{ts} and η_{t} one deals with the prefactor r_0, which is equated to ν_{t}, in the framework of the transition state theory approximation used here (see section 6.2)

There are four dimensionless parameters which, together, determine in which regime of friction or slipperiness the system slides. The first of these is the Tomlinson-like parameter

$$\gamma_{\mathrm{eff}} = \frac{2\pi^2 U_0}{k_{\mathrm{eff}} a^2}, \tag{5}$$

reminiscent of the key parameter in the traditional one-spring model, in the present case with the effective spring coefficient $k_{\mathrm{eff}} = (k^{-1} + K^{-1})^{-1}$. It determines the number of potential wells accessible to the tip apex for a fixed position of the support, provided the cantilever position is adjusted to keep equal forces in both springs. This quasistatic description is appropriate only when the system sticks in the interaction potential wells. When $\gamma_{\mathrm{eff}} < 1$ there are no mechanical instabilities in the system, and it will exhibit continuous, near-frictionless sliding, i.e. SL. If $\gamma_{\mathrm{eff}} > 1$ instabilities are possible and their manifestation will depend on the other three parameters.

The second parameter is γ, as defined by equation (2), which determines the number of surface wells accessible to the tip apex for a fixed position of the cantilever. This parameter is important, since $m \ll M$, which makes the motion of the apex fast with respect to that of the cantilever. Hence this is the appropriate Tomlinson parameter to characterize the potential landscape experienced by the apex in any dynamical process, whether it is straightforward slipping or a more complex process involving thermally activated jumps.

If $\gamma > 1$ and, hence, activated jumps are possible, a relative measure for the average number of these jumps per lattice spacing traveled by the support is provided by the third dimensionless parameter,

$$\beta = \frac{\widetilde{r}}{V/a} = \frac{a}{V}\sqrt{\frac{k}{m}} \exp\left(-\frac{U_0}{k_{\mathrm{B}} T}\right). \tag{6}$$

This parameter is no more than indicative, as the actual potential energy landscape experienced by the apex depends on the cantilever position; the barriers can both be smaller and larger than U_0, and in certain situations they can be much smaller than U_0.

Finally, if β is large enough (at a sufficiently weak potential energy corrugation, at high temperature, or at low velocity) the fourth important parameter comes into play,

$$\Gamma = \frac{2\pi^2 \overline{U}_0}{K a^2}, \tag{7}$$

with $\overline{U}_0$ the corrugation of the effective tip–surface interaction, averaged over the rapid thermal motion of the apex. It characterizes the number of wells accessible to the cantilever for fixed support position in the effective potential energy landscape. Also this parameter should be considered as a mere indication, since expression (7) implies a sinusoidal potential while the effective potential is periodic but generally not sinusoidal (see figure 3 in [28]). Examples of calculated effective interaction potentials are given in [28, 32].

We have seen that within the two-mass-two-spring description the system is characterized by three Tomlinson-like parameters, given by equations (2), (5) and (7), instead of the single parameter, equation (5), of the traditional one-spring model. Note that neglecting thermally activated motion, one would have $\overline{U}_0 = U_0$ and, hence, $\gamma_{\text{eff}} = \gamma + \Gamma$.

Since two of the four above parameters are only indicative, they do not allow one to determine strict boundaries between all regimes of friction, but they are useful for a qualitative classification.

4.2. Regimes

In this subsection, we present a brief inventory of the seven sliding regimes that we have encountered in our calculations, classified in terms of the four dimensionless parameters, introduced above. A detailed view of each of these regimes will be provided in the calculation results of section 5.

If $\gamma > 1$ and, hence, $\gamma_{\text{eff}} > 1$, the traditional one-spring model predicts dissipative SS motion. By surprising contrast, the two-mass-two-spring model introduces several essentially different, and not necessarily dissipative, regimes.

4.2.1. Ordinary stick-slip (SS). If $\gamma > 1$ while β is so small that thermally activated jumps of the tip apex play only a minor role, the system will be in the *ordinary SS regime*.

4.2.2. Stochastic stick-slip (SSS). If $\gamma > 1$ while β is not too small, so that there are two or several thermally activated jumps of the tip apex back and forth during the time $(\frac{a}{V})$ required for traveling one lattice spacing, one expects the system to exhibit a variety of stochastic types of behavior, depending on the precise values of the parameters involved. In particular, *SSS* can manifest itself as seemingly usual SS but with 'structured' slips, which are accompanied by several jumps of the tip back and forth between the accessible potential wells (one of the cases considered in [32]).

4.2.3. Stuck in slipperiness (SinS). If $\gamma > 1$, and β is sufficiently large to provide rapid thermally activated motion of the tip apex between the accessible potential wells, and $\Gamma > 1$, the system can be in the strongly counterintuitive regime considered in [28]: one observes seemingly usual SS motion of the cantilever in spite of a complete delocalization of the tip–surface contact over the allowed positions. Comparing equations (2) and (7) and taking into account that the corrugation of the potential in this case should be relatively small and, generally, $\overline{U}_0 < U_0$, one understands that the SinS regime requires limited K values, i.e. systems

with a sufficiently soft cantilever, such as the Leiden FFM, which typically operates with $K < 10\,\mathrm{N\,m^{-1}}$. In this SinS regime friction is low but nonzero.

4.2.4. Thermolubricity (TL). If $\gamma > 1$, and β is sufficiently large to provide complete delocalization of the contact as in the previous case, but $\Gamma < 1$ (relatively hard cantilever), the system will exhibit continuous, near-frictionless sliding of the cantilever in the effective potential averaged over the rapid, thermally activated motion of the tip apex. We refer to this regime as TL, since this is a kind of SL, but reached at $\gamma_{\mathrm{eff}} > 1$ due to thermal activation.

4.2.5. Slipping via an intermediate position (SIP). If $\gamma \gtrsim 1$ (close to unity) the tip apex experiences two potential wells only in a narrow range of cantilever positions, outside of which it sees only a single well. In this case, the potential barrier between the two wells is substantially smaller than U_0. As a result, the contact can be delocalized in this two-well region, even at relatively high values of the interaction potential corrugation. The consequence of this partial delocalization is remarkable and highly counterintuitive. The cantilever can be observed to pass through an intermediate, 'stable' position during its slipping from one well to the next, as if there were an intermediate lattice position between the two wells. The physics behind this phenomenon has been recently considered by us in detail elsewhere [32]. In brief, the apparent intermediate state is related to a flattening of the maxima in the effective interaction potential, sensed by the cantilever. This should be viewed as an entropic effect caused by the distribution of the tip apex over the two adjacent local optima in the potential that it experiences itself. This regime occurs both for hard cantilevers (one of the cases considered in [32]) and for soft cantilevers (see below). Friction is nearly zero in this case. To a certain extent, we can consider this situation as a specific kind of TL.

4.2.6. 'Passive apex (PA)' regime. An interesting situation arises in a narrow range of the parameters involved, when $\gamma_{\mathrm{eff}} > 1$ but $\gamma < 1$. The tip apex can neither jump nor slip by itself, but dynamical instabilities in the whole, two-mass system can take place. In this case, the system will exhibit a kind of SS motion, in which the apex moves together with the cantilever on the time scale characteristic for the entire mass. In this regime the apex should be regarded as passive, indeed; all previous regimes featured a more active role of the apex: it either directly initiated slips of the cantilever (SS and SSS) or generated the effective potential for the cantilever (SinS, TL and SIP).

4.2.7. Superlubricity (SL). One boundary between regimes is well defined, namely $\gamma_{\mathrm{eff}} = 1$. In all previous regimes we had $\gamma_{\mathrm{eff}} > 1$. If, on the other hand, $\gamma_{\mathrm{eff}} < 1$, there are no dynamical instabilities and the system will exhibit continuous, near-frictionless sliding, the regime is often called SL.

5. Traversing friction regimes by varying the corrugation of the interaction potential

Having already introduced the seven different friction regimes in the previous section, we now turn to the two series of examples that illustrate all of them in more detail. According to equations (2), (6) and (7), the selection of the specific friction regime should sensitively depend on U_0, K and a. Let us investigate how the behavior evolves when we vary the corrugation of the

interaction potential U_0 in systems with different combinations of the cantilever stiffness K and the lattice period a. In experiments there are several ways to vary U_0. The potential corrugation is determined by the material pair of tip and substrate, the effective contact area, the contact force and the (relative) crystallography of the contacting surfaces. U_0 can be varied easily for example by adjusting the normal force on the contact [11] or by adjusting the relative lattice orientation of the contact [10]. In addition to this, in actual experiments different scan lines often correspond to different potential corrugations, so that a variation in potential is often realized in practice within a single lateral force image (2D FFM scan of the surface).

We first specify the parameters, of which the values are relatively certain. The tip stiffness k is in the order of several Newtons per metre, as typically observed in FFM experiments and justified by our recent calculations [28]. The effective mass of the tip apex is $m \sim 10^{-20}$ kg, as calculated in [28], and the typical cantilever mass M is in the range from 10^{-11} to 10^{-8} kg. The specific value of M is not very important as long as we consider scanning velocities V in the range from several nanometres per second to several tens of nanometres per second, typical for FFM. The temperature is $T = 300$ K, as in almost all FFM experiments performed up to now.

At this point, at least three essentially different types of systems can be recognized. We will refer to these three cases as (i) 'soft cantilever', (ii) 'hard cantilever' and (iii) 'large lattice spacing'. The differences between these three cases are in how the behavior evolves with reducing U_0, from ordinary SS motion to SL: (i) via SinS, (ii) via TL, (iii) nearly directly. In the following, we provide a qualitative description for each of these three situations, which will be complemented by computations performed using the hybrid numerical algorithm described above. In addition to visualizing the anticipated regimes, the numerical calculations lead to several additional, sometimes surprising observations.

5.1. 'Soft cantilever' (SS→SinS→SL)

If K is sufficiently small, e.g. $K = 6\,\mathrm{N\,m^{-1}}$, and a is not too large, e.g. $a = 0.25$ nm, there will be a range of interaction potential amplitudes, for which γ is substantially larger than unity (multi-well contact), while thermally activated jumps of the apex are rapid and provide contact delocalization, generating an effective potential for the cantilever with $\Gamma > 1$. These are the conditions for the SinS regime. A system with such a K, a-combination should be expected to evolve, with reducing U_0, from ordinary SS motion to the SinS regime and further to SL.

These expectations are confirmed by our numerical calculations. The mean friction force as a function of potential corrugation, computed for a soft cantilever with $K = 6\,\mathrm{N\,m^{-1}}$ and with typical values for the other parameters is shown in figure 3 (solid squares and solid curve). Clearly, the shape of the friction-versus-corrugation curve suggests the presence of several friction regimes. The high corrugations necessarily correspond to SS motion, for which a nearly linear dependence is expected. The low corrugations necessarily result in SL, i.e. nearly zero friction. The low, but nonzero values in the intermediate regime correspond to SinS behavior, for which only a weak dependence has been predicted on the corrugation of the interaction potential (see figure 3 in [28]). A more detailed view of the friction regimes involved is given in figure 4, where the measured lateral force between support and cantilever, $F = K(Vt - X)$, and the tip apex position relative to that of the support, $(Vt - x)/a$, are shown as functions of the support position, Vt/a, for various potential corrugations.

At high corrugations, of the order of or above 0.5 eV, the system is in the ordinary SS regime, which is illustrated in figure 4(A-1) for $U_0 = 0.7$ eV. The other two panels at

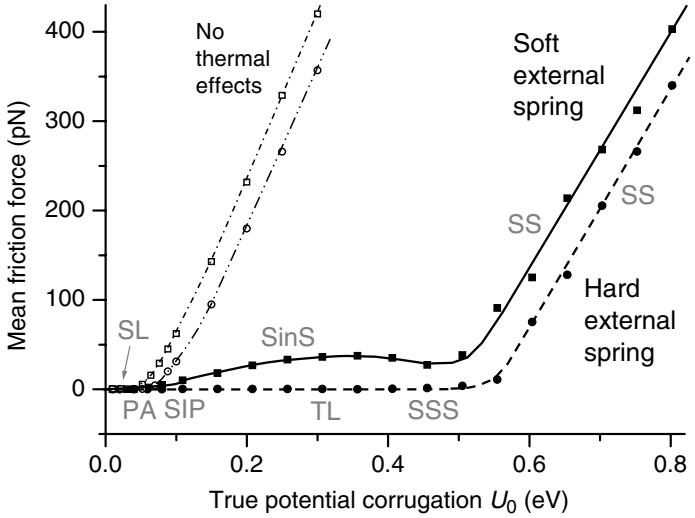

Figure 3. Mean friction force as a function of the corrugation of the interaction potential, calculated for $k = 3\,\mathrm{N\,m^{-1}}$, $a = 0.25\,\mathrm{nm}$, $V = 10\,\mathrm{nm\,s^{-1}}$, $m = 1 \times 10^{-20}\,\mathrm{kg}$, $M = 1 \times 10^{-9}\,\mathrm{kg}$, and for $K = 6\,\mathrm{N\,m^{-1}}$ (squares) or $K = 60\,\mathrm{N\,m^{-1}}$ (circles). Open symbols are in absence of thermal effects—equivalent to the traditional Tomlinson model—and solid symbols are for a temperature of $T = 300\,\mathrm{K}$. All friction forces have been averaged over a sliding distance of 10 lattice spacings. The lines are meant to guide the eye. Thermal noise on the cantilever motion has been switched off. Different regimes of friction are indicated: ordinary stick-slip (SS), stochastic stick-slip (SSS), stuck in slipperiness (SinS), thermolubricity (TL), slipping via an intermediate position (SIP), 'passive apex' regime (PA) and superlubricity (SL).

0.7 eV provide a more detailed view of the slip event. The apex slips on the timescale of ν_t^{-1} (figure 4(A-3)), while the cantilever slips (and oscillates) with a characteristic time of ν_c^{-1} (figure 4(A-2)), as expected. Even though figure 4(A) is fully in the SS regime, the motion is already affected noticeably by thermal effects. Every slip event is initiated by a pre-critical jump of the tip apex, which necessarily always occurs at a point before the mechanical slip instability, the precise timing being distributed stochastically. This is clearly seen in the irregular timing of the slip events in figure 4(A-1). It is also reflected in the scatter in the mean friction values at high corrugations, calculated for the soft cantilever in figure 3. Each value in figure 3 represents the average friction force over a limited number of atomic spacings passed by the system (ten in this case); the scatter is removed by averaging over a sufficiently long path.

At lower corrugations the system enters an intermediate regime, in which several thermally activated jumps of the apex, back and forth between the accessible potential energy wells, occur per lattice spacing traversed by the support (figure 4(B-3)). Surprisingly, these multiple jumps do not lead to the introduction of significant 'noise' (randomness) in the cantilever motion. Instead, the cantilever exhibits very regular SS behavior (figure 4(B-1)) with only weak fluctuations superimposed (figure 4(B-2)). In fact, under these conditions the cantilever motion is even more regular than in the case of ordinary SS motion (compare with figure 4(A-1)). The explanation for this is as follows. At higher corrugations, in the SS regime, the tip apex jumps precisely

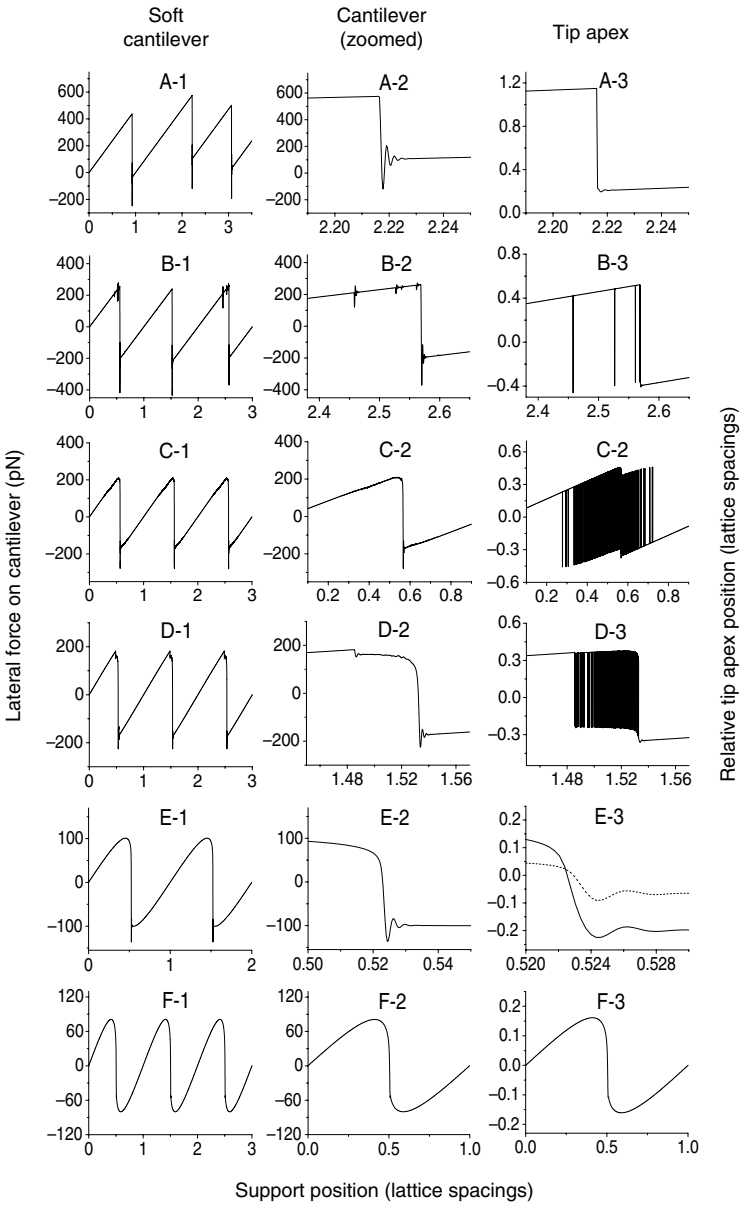

Figure 4. Evolution of the friction behavior—lateral force and relative tip position against support position, Vt/a— for a soft cantilever with $K = 6\,\mathrm{N\,m^{-1}}$ and with all other parameters as in figure 3. Calculation results are shown for U_0-values of 0.70 (A), 0.45 (B), 0.20 (C), 0.13 (D), 0.05 (E) and 0.04 eV (F). The left column shows the measured forces $F = K(Vt - X)$ between support and cantilever. The middle column shows the interesting slip region in more detail. The right column shows the position of the tip apex relative to the support, $(Vt - x)/a$, in the same region of interest. The dotted curve in panel E-3 shows the position of the cantilever relative to the support and indicates that under those conditions it faithfully follows the apex motion. Thermal noise on the cantilever motion has been switched off in order to better visualize the inherent dynamics of the system. Note that the time resolution in the plotted tip apex positions in the right-hand panels of (B), (C) and (D) is too coarse to display all calculated jumps.

once per lattice period and, because of thermal excitations, it always jumps too early. As a result the cantilever experiences a pattern of forces that is irregular and always a bit shifted with respect to the substrate lattice. It therefore also jumps too early and with clear noise on the timing of the jumps. When the potential is lowered and backward jumps become frequent, i.e. when one enters the intermediate regime, the backward jumps in a way 'correct' the wild behavior of the apex. When it has jumped forward much too early, there is a high probability for a reverse jump, occurring before the slow cantilever has been able to respond to the temporarily advanced apex position. As a result, the effective potential experienced by the cantilever, which reflects the average behavior of the tip apex, is not only made more regular again, but it is also shifting back again in the direction of the original lattice positions. Although U_0 is slightly lowered in this scenario, $\overline{U}_0$ actually grows slightly. The reason is that the effect of lowering U_0 goes exponentially into the backward jump rate and therefore has a super-linear effect in the increase of $\overline{U}_0$ that is larger than the direct decrease in U_0. One should regard the entire range of potential corrugations in figure 3 between 0.25 and 0.55 eV as the transition between the SinS regime and the SS regime. Only at and below 0.25 eV, we find true SinS behavior and only above 0.55 eV, we find true SS behavior. The weak local maximum in F around 0.35 eV and the minimum around 0.45 eV in figure 3 form the signature of the crossover between these two regimes.

At a low corrugation U_0 of 0.20 eV, the system is fully in the SinS regime (figure 4(C)). Although for the set of parameters used in this calculation the contact delocalization does not occur for all support positions (see figure 4(C-3)), its effect is already sufficient for the cantilever to experience a smooth and highly regular effective potential, to which it responds with very regular SS motion (figure 4(C-1)). Note that, as in figure 2(C), slipping of the cantilever takes place within the range of support positions for which the apex is delocalized (compare figures 4(C-2) and (C-3)).

At even lower corrugation, the multi-well situation for the tip apex and therefore the contact delocalization is restricted to an increasingly narrow region of support positions (figure 4(D-3)). This manifests itself in the very specific type of SS motion of the cantilever, with 'structured' slips (figures 4(D-1) and (D-2)), already mentioned in section 4.2.5. Depending sensitively on the values of U_0, k and a, this fine-structure can appear as a gradual slipping (figure 4(D-2)) or as a slipping via a well-defined, intermediate position. The latter behavior is visible vaguely in figure 4(D-2) and very prominently in the calculation results for a hard cantilever, shown in figures 5(E-1) and (E-2) (to be further discussed below).

The 'PA' regime, anticipated in section 4.2.6 for $\gamma < 1$ and $\gamma_{\text{eff}} > 1$, is realized in a narrow range of low corrugations. At every cantilever position, only a single potential well is accessible to the tip apex. Nevertheless, the apex and cantilever perform SS motion (see figures 4(E-1) and (E-2)). Here, we encounter an interesting manifestation of the complex two-mass-two-spring dynamics. The apex, while rapidly exploring its surroundings under other circumstances, in this case has no choice but to follow the slow motion of its 'big partner' (see figure 4(E-3), where the behavior of the cantilever-support distance is shown additionally by the dashed line).

When the corrugation of the potential is further lowered to reach the critical value corresponding to $\gamma_{\text{eff}} = 1$ (0.04 eV in this example), only a single potential well is available to the tip apex for every cantilever position and only a single potential minimum is available to the cantilever for every support position, so that all SS type instabilities disappear and the system goes over to continuous, near-frictionless sliding, i.e. SL, as seen in figure 4(F).

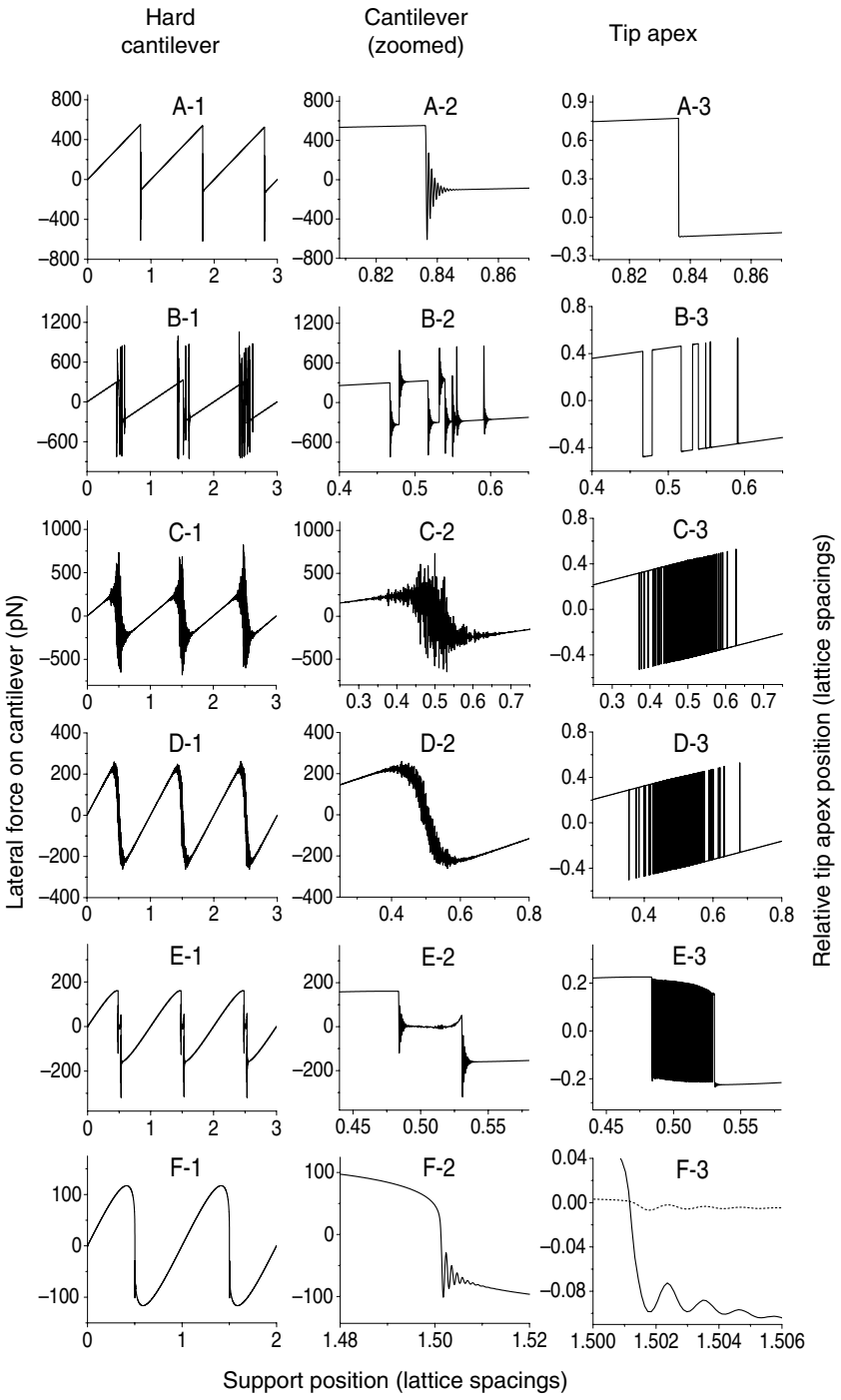

Figure 5. Similar to figure 4, but for a hard cantilever with a spring coefficient of $K = 60\,\mathrm{N\,m^{-1}}$. Calculation results are shown for U_0-values of 0.70 (A), 0.50 (B), 0.35 (C), 0.25 (D), 0.08 (E) and 0.058 eV (F). The dotted curve in panel (F-3) shows the position of the cantilever relative to the support and indicates that under those conditions it faithfully follows the apex motion. Note that the time resolution in the plotted tip apex positions in the right-hand panels of (C), (D) and (E) is too coarse to display all calculated jumps.

5.2. 'Hard cantilever' (SS→TL→SL)

If K is large, the case of traditional SS can be reached only for high γ-values. In the lower range of potential corrugations, with γ larger than unity but low enough that the contact is completely delocalized, one always has $\Gamma < 1$, so that the cantilever slides continuously. This is the regime referred to as TL. Such a system will go, with reducing U_0, from ordinary SS motion, via a regime of SSS motion, to TL and further to SL. Again, the transition to SL, at γ close to unity, can proceed via SS motion through intermediate positions (section 4.2.5) and the 'PA' type of SS (section 4.2.6).

We recognize this sequence of friction regimes in the numerical calculations. The mean friction force as a function of the potential corrugation, calculated for a high cantilever spring coefficient, $K = 60\,\mathrm{N\,m^{-1}}$, and with all other parameters equal to those for the previous case of the soft cantilever, is shown in figure 3 by the solid circles and the dashed line. In a narrow range of corrugations around 0.55 eV, the friction forces show a transition from finite values, characteristic for SS motion, to near-zero friction. Since this transition takes place well above the transition at 0.056 eV to SL, it suggests a more than pronounced role of thermal effects in the case under consideration.

The full variety of regimes for the hard cantilever is shown in figure 5. At corrugations above 0.55 eV the system is seen to be in the ordinary SS regime (figure 5(A)). The motion is more regular than in the case of the soft cantilever (figure 5(A-1)), which is also indicated by the smaller scatter on the mean friction force values in this regime (figure 3), compared to the soft cantilever. The dynamics of slipping has been found in all calculations to be similar to that of the soft system, without noticeable qualitative differences.

Around 0.5 eV the system is in an intermediate regime where several activated jumps of the tip apex occur per lattice spacing scanned (figure 5(B-3)). The hard cantilever is capable of following these apex jumps completely (figure 5(B-2)), so that it exhibits SSS motion, with very pronounced, multiple forward and reverse jumps (figure 5(B-1)). This produces a nearly zero mean friction force, as seen in figure 3. One meets here an essential difference with the previous case of a soft cantilever (see figure 4(B)), for which ordering of the motion of the system was observed in the intermediate regime rather than disordering. Two consequences of the difference in the K-value conspire to generate this difference in behavior. These are the difference in cantilever eigenfrequency and the difference in the distance over which the cantilever has to slip in response to a jump of the tip apex over one lattice spacing a. This distance is inversely proportional to K.

At lower corrugations the system goes over to TL (figures 5(C) and (D)). Strong delocalization of the contact in a range of support positions (figures 5(C-3) and (D-3)) leads to the formation of an effective potential for the cantilever, the corrugation of which turns out to be relatively weak with respect to K, so that $\Gamma < 1$. Consequently, in contrast to the case of small K, the system does not exhibit any SS-like instability but continuous, albeit 'noisy', sliding (figures 5(C-1), (C-2), (D-1) and (D-2)) with nearly zero friction—TL. It is remarkable that this noise can be modest (figures 5(D-1) and (D-2)) or very strong (figures 5(C-1) and (C-2)), sensitively depending on the corrugation of the interaction potential. In all cases this represents the response of the cantilever to the rapid jumps of the apex. The strong noise in figures 5(C-1) and (C-2) is due to incomplete averaging, which brings the system to an intermediate situation between the case of figure 5(B), where the cantilever completely follows the tip apex, and the case of figure 5(D), where the cantilever averages over the large number of rapid apex jumps.

Upon a further decrease of the corrugation, one restricts the contact delocalization to a narrow region of support positions (figure 5(E)). Figures 5(E-1) and (E-2) illustrate the stunning consequence of this, in the form of cantilever slipping via a well-established, intermediate position, as discussed and explained above. In a narrow interval of lower corrugations, for which $\gamma < 1$ and $\gamma_{\text{eff}} > 1$, we observe 'PA' behavior, with slipping initiated by the cantilever and followed faithfully by the tip apex (figure 5(F); the dashed line in figure 5(F-3) indicates the behavior of the cantilever). Finally, when $\gamma_{\text{eff}} < 1$ the system exhibits complete SL, with curves similar to those in figure 4(F) (not shown here).

5.3. 'Large lattice spacing' (SS→SL)

The simplest scenario of a direct transition from SS motion to SL is met for relatively large lattice spacings (note that a appears squared in equation (2)). In this case a multi-well contact, i.e. $\gamma > 1$, can be realized only at high amplitudes of the interaction potential and thermal effects are limited with respect to the two previous cases considered (soft and hard cantilevers, combined with typical lattice spacing). The case of large lattice spacings has been recently considered elsewhere [32], so we do not reproduce the details of our calculations here. In brief, on the way from ordinary SS motion to SL, with decreasing potential corrugation, the system passes through SS behavior with 'structured' slips of several types. First, at higher corrugation, there are slips accompanied by several forward and reverse jumps, similar to the behavior in figure 5(B). Then, at lower corrugations, for which γ is close to unity, there are gradual slips and slips via an apparent, intermediate state, similar to the cases in figures 4(D) and 5(E).

6. Discussion

6.1. Modest role of thermal noise on the cantilever

Thermal noise on the cantilever motion has been switched off in the calculations of figures 3–5, discussed above ($\eta_{\text{n}} = 0$, in the noise term in equation (4)), in order to visualize the inherent dynamics of the system. The somewhat noisy behavior seen in some of the graphs of the second column in figures 4 and 5, especially in figure 5(C-2), reflects the response of the cantilever to the thermally activated jumps of the tip apex, i.e. 'indirect' thermal noise.

When the random force in the Langevin equation for the cantilever (equation (4)) is switched on ($\eta_{\text{n}} \neq 0$), the average behavior of the system, shown in figure 3, remains almost completely unchanged, while the instantaneous lateral force of course acquires fluctuations (see, e.g., figures 2(A) and (C)). Not only do these fluctuations mask the fine structure in the slip events seen in figures 4 and 5—depending on η_{n}, this is a modest or a strong effect—they also make this structure somewhat more complex and variable from one lattice position to another one. This is because thermally induced changes in the cantilever position modify the potential profile felt by the tip apex and, hence, affect the occurrence of its activated jumps, which, in turn, is reflected in the detailed behavior of the system as a whole.

6.2. Dramatic role of thermally activated tip apex jumps

In contrast with the modest role of cantilever fluctuations, the thermal noise on the position of the tip apex is essential. In our calculations, it is embodied by the thermally activated jumps. The thermal noise and damping of the tip apex motion, interrelated by the fluctuation–dissipation

theorem, reflect themselves in the value of the pre-exponential factor r_0 in the jump rate in equation (3). In our case, the traditional transition state theory approximation for the prefactor ($r_0 = \nu_t$) implies the damping factors for the tip apex motion with respect to the cantilever (i.e. to the rest of the tip) (η_t) and with respect to the surface (η_{ts}) to be comparable with the characteristic frequency of the tip apex, $\eta_t \sim \eta_{ts} \sim \nu_t$.

If there were no thermally activated jumps of the tip apex, i.e. $r_{ij} = 0$, the two-spring description would be fully equivalent to a one-spring description [28]. The corresponding behavior of the mean friction force as a function of the corrugation of the potential is shown by the open symbols and the dash-dot and dash-dot-dot curves in figure 3. The same results can be obtained by considering very low temperatures or, formally, assuming a very high value of the effective mass m.

Instead, thermally activated motion of the tip apex plays a truly dramatic role in friction at room temperature, as a consequence of the ultra-low ($\sim 10^{-20}$ kg) effective mass. As seen from figure 3, it leads to an order-of-magnitude decrease of friction in the range of corrugations $U_0 < 0.5$ eV, both in the cases of a soft and a hard cantilever. This dramatic suppression of friction directly reflects the delocalization of the tip–surface contact, which leads either to low-dissipation SS motion (SinS regime) or to continuous sliding (TL), depending on the cantilever stiffness K.

At higher corrugations, $U_0 > 0.5$ eV, the relative effect of thermal activation is seen to decrease with increasing corrugation, but it remains pronounced. There, in the ordinary SS regime, the decrease of the mean friction force is accompanied by two effects: a decrease of the maximal lateral forces reached prior to each slip event and a change in the shape of the SS patterns, which become more symmetric with respect to the sliding direction. Both effects are due to a single reason: thermal activation of slip events that always take place at support positions somewhat preceding those where the system would be mechanically instable. The physics of these pre-critical jumps was already fully captured by the one-spring model, as described in section 1, but in our case the effect is dramatically strong, in view of the extremely high prefactor associated with the ultra-low effective mass. For instance, at $U_0 = 0.7$ eV, the maximum lateral force is about 500 pN, both for a soft and for a hard cantilever (see figures 4(A) and 5(A)), while the prediction of the Tomlinson model without thermal effects ($F_{max} = \frac{\pi U_0}{a}$) would be as high as 1400 pN.

Another remarkable manifestation of thermal effects is that in the case of a hard cantilever the transition from SS to continuous, near-frictionless sliding starts already at a corrugation of about 0.55 eV (see figure 3), which is approximately a factor ten higher than the critical corrugation for the transition to straightforward SL (0.056 eV for $K = 60\,\mathrm{N\,m^{-1}}$). There is a surprisingly wide range of potential corrugations with TL, which separates the SS and SL regimes in this case. Importantly, the rounded force-versus-position patterns in the TL regime (figure 5(D-1)) look very similar to those characteristic for the SL regime (figure 4(F-1)); when thermal noise is switched on they become indistinguishable.

Note that the thermally-induced suppression of friction was predicted by us before [16] in the framework of the one-spring-one-mass model. Assuming a sufficiently high value of the prefactor of thermally activated jumps of the single, effective mass, a friction-versus-corrugation relation had been predicted that mimicked the solid curve in figure 3, albeit that it was completely monotonous. This curve provided a reasonably good fit to the experiments [10, 25], but, as has already been mentioned in section 1, it is not easy to explain the origin of pronounced thermal activation within the one-spring model with a macroscopically large

effective mass. This problem is completely fixed within the two-spring model with the ultra-low effective mass m. Indeed, now the suppression of friction results from pronounced thermally activated jumps of the tip apex, which are very natural for a nearly atomically small object. Thermal activation in the cantilever motion plays only a minor role, as could be expected for an object of macroscopic mass. This is directly seen from the very regular character of the SS patterns in the SinS regime (figures 2(C) and 4(C-1)).

6.3. Role of the cantilever stiffness

It is instructive to compare the cases of soft and hard cantilevers, keeping in mind that both types are used in modern FFM experiments [10, 11, 13, 25]. As seen in figure 3, to first approximation the behavior of the mean friction force is similar for the two cases: low friction at corrugations U_0 below 0.5 eV, and a linear increase of friction at higher corrugations. Our calculations show that the quantitative differences between the mean friction forces for soft and hard cantilevers are even smaller at a lower value of the tip stiffness, $k = 2\,\mathrm{N\,m^{-1}}$, than for the value of $k = 3\,\mathrm{N\,m^{-1}}$ used in figure 3, in the full range of U_0-values considered.

In spite of this quantitative similarity, there are a number of principal differences in the detailed dynamics of the systems with soft and hard cantilevers, as illustrated by figures 4 and 5. In the region of low corrugations, $U_0 \sim 0.1$–0.3 eV, the contact is delocalized, thus presenting an effective interaction potential to the cantilever, by averaging over the rapid thermal motion of the tip apex. The corrugation of this effective potential turns out to be sufficient for the system with the soft cantilever to cause seemingly usual SS motion (SinS, figure 4(C)), with low but nonzero friction. For a hard cantilever, the same effective corrugation is too weak to produce mechanical instabilities in the system, which therefore exhibits continuous, near-frictionless sliding (TL, figure 5(D)). The transition from SinS behavior to TL with increasing cantilever stiffness K has been demonstrated before in figure 4 of [28].

At intermediate corrugations, when a limited number of activated jumps of the tip apex occur per lattice spacing passed, the soft cantilever does not follow each of them but exhibits very regular SS motion (figure 4(B-1)). In contrast, the hard cantilever manages to follow the jumps of the apex, as explained above, thus performing highly SSS motion (figure 5(B)). We see that also in this narrow region of corrugations, the dynamics of the soft and hard systems are essentially different.

At high corrugations, $U_0 > 0.5$ eV, in the ordinary SS regime, the difference in behavior is the other way around. Now, there is much more irregularity in the SS motion of the soft system than in that of the hard system (compare, e.g. figures 4(A-1) and 5(A-1)). Also, this manifests itself in figure 3, where the scatter in the calculated values of the mean friction force is larger for the soft system than for the hard one.

6.4. Towards the reinterpretation of experiments

Serious reinterpretation of many seemingly standard FFM experiments will be needed. As follows from the discussion above, this reconsideration should include the actual regime of friction, the lateral force amplitude, the true corrugation of the tip–substrate interaction energy landscape, the slip times and the thermal noise. Also, the tip stiffness (k) should be carefully readdressed, since its relation with the initial slope in the plot of lateral force versus support position is more complex in the two-spring model than in the one-spring model—this point

has not been touched upon in this paper. Further theoretical investigations will be required to relate the physical parameters of the system with the observables. At this stage several general statements can be made.

Firstly, as directly seen from figure 3, in typical FFM experiments [10, 11, 13, 25], in which friction forces in the range 0–500 pN have been measured, the true corrugation of the tip–surface interaction potential has not been in the range 0–0.4 eV as was concluded from the observed maxima in the lateral force, but rather in the range 0.5–1 eV. Such an error by a factor of 2–3 in the amplitude of the interaction potential is, no doubt, dramatic.

Secondly, the interpretation of the transitions from SS to continuous sliding recently observed in experiments with essentially different cantilevers [10, 11] should be changed completely. Interpreted within the context of the traditional one-spring model, the hard system [11] appeared to exhibit a transition from SS motion to trivial, mechanical superlubricity, while the soft system appeared to experience 'TL' in between [16]. The above calculations within the two-mass-two-spring approach suggest the opposite. The hard system must have gone through the transition from SS to TL. This is supported by the direct similarity between the force loops reported in [11] and the behavior seen in figure 5(A-1) and, most importantly, figure 5(D-1). The soft system should have made the transition from ordinary SS motion to the low-friction, SinS regime, possibly masked by the thermal noise in the experiment [10]. Whether or not the trivial, mechanical SL ($\gamma_{\text{eff}} < 1$) has been reached in both experiments remains unclear at this point.

Thirdly, the observations made above with respect to the SS irregularities in the soft and hard systems provide a good hint to understand why all experiments performed with the soft Tribolever® systematically demonstrated more 'noisy' results than those carried out with more conventional, hard cantilevers. An order of magnitude difference in the cantilever stiffness in the two-spring system has been shown above to lead to a significant difference in the stochastic nature of the observations, indeed. Note that the cantilever mass was fixed in our calculations, while in the experiments under discussion it differed by nearly three orders of magnitude. This can additionally contribute to the difference in noise.

7. Concluding remarks

In summary, we have explored the dynamics of FFM measurements in the framework of a two-mass-two-spring description of the experiment. One of the springs corresponds to the traditional cantilever stiffness, while the other represents the compliant FFM tip. Although the spring coefficients of these two springs typically differ by no more than two orders of magnitude, the masses effectively loaded on these springs are extremely different, basically being macroscopic for the cantilever and nearly atomic for the separately moving, apex part of the tip. This results in very different timescales in the combined spring system, which leads to a wealth of partly unsuspected friction phenomena. In this paper, we have categorized these friction regimes and we have illustrated and analyzed them in detail with the use of a hybrid computational scheme, involving Langevin dynamics for the slow cantilever motion and a Monte-Carlo treatment of the rapid motion of the tip apex.

Although the explicit introduction of the second spring and the associated rapid timescale has made this approach much more realistic than the traditional, single-spring description of FFM experiments, several important elements are still missing from our calculations. In particular, the potential energy landscape and the motion of the tip apex and cantilever were all assumed to be strictly 1D. In practice, the tip apex will almost always take advantage of

essentially 2D, low-barrier pathways through the interaction potential. Even in the case of highly different cantilever stiffnesses in the two lateral directions, as is typical for most cantilevers, the tip compliance will be quite similar for the two directions. Further calculations are planned that will incorporate 2D effects. In spite of this obvious omission in our present calculations, the excellent agreement that we have obtained with recent experiments strongly suggests that we have identified all or nearly all relevant nanoscale friction regimes.

It is important to realize that we have not only recognized different scenarios for the motion of the tip apex over the surface and for the motion of the cantilever with respect to the support and with respect to the tip apex, but that each of these scenarios also represents a different mechanism for energy dissipation, i.e. a different form of friction. In principle, numerical fits with our model to measurements staged in different friction regimes should allow one to determine the truly microscopic friction parameters, such as the amplitude of the interaction potential and the microscopic damping coefficients, especially that of the rapidly moving tip apex.

Most calculations presented in this paper have been carried out for a single velocity. Yet, as indicated by the parameter β, the velocity has a direct influence on the average number of thermally activated tip apex jumps per lattice spacing traveled. Preliminary calculations of the velocity dependence indicate a more complex and interesting behavior than predicted earlier within the traditional single-spring model.

We repeat our conclusion that the nanotribology community will have to reconsider the interpretation of many seemingly standard friction force microscopy measurements, including a wide variety of results that have been published already.

In conclusion, we speculate that the effects highlighted here for the case of an FFM tip in contact with a substrate can possibly also play a role in the much more general context of the asperities that establish the contact between two sliding bodies. In other words, there may be much more thermally driven dynamics in macroscopic sliding due to the local compliance of the contacting surfaces than we have ever imagined.

Acknowledgments

We are grateful to Daniel Abel and Joshua Dijksman for significant contributions and substantial help in the early stages of this investigation. This work is part of the research program of the ‘Stichting voor Fundamenteel Onderzoek der Materie (FOM)’ and was made possible by financial support from the ‘Nederlandse Organisatie voor Wetenschappelijk Onderzoek (NWO)’.

References

[1] Dowson D 1998 *History of Tribology* 2nd edn (London: Longman)
[2] Feynman R P 1977 *Lectures on Physics I* 6th edn (Reading, MA: Addison-Wesley)
[3] Persson B N J 1998 *Sliding Friction: Physical Principles and Applications* (Berlin: Springer)
[4] Carpick R W and Salmeron M 1997 *Chem. Rev.* **97** 1163
[5] Urbakh M, Klafter J, Gourdon D and Israelachvili J 2004 *Nature* **430** 525
[6] Mate C, McClelland G, Erlandsson R and Chiang S 1987 *Phys. Rev. Lett.* **59** 1942
[7] Prandtl L 1928 *Z. Angew. Math. Mech.* **8** 85
[8] Tomlinson G A 1929 *Phil. Mag.* **7** 905

[9] Hirano M, Shinjo K, Kaneko R and Murata Y 1991 *Phys. Rev. Lett.* **67** 2642
Hirano M, Shinjo K, Kaneko R and Murata Y 1997 *Phys. Rev. Lett.* **78** 1448
[10] Dienwiebel M, Verhoeven G S, Pradeep N, Frenken J W M, Heimberg J A and Zandbergen H W 2004 *Phys. Rev. Lett.* **92** 126101
[11] Socoliuc A, Bennewitz R, Gnecco E and Meyer E 2004 *Phys. Rev. Lett.* **92** 134301
[12] Müser M H, Urbakh M and Robbins M O 2003 *Adv. Chem. Phys.* **126** 187
[13] Gnecco E, Bennewitz R, Gyalog T, Loppacher Ch, Bammerlin M, Meyer E and Güntherodt H-J 2000 *Phys. Rev. Lett.* **84** 1172
[14] Dudko O K, Filippov A E, Klafter J and Urbakh M 2002 *Chem. Phys. Lett.* **352** 499
[15] Reimann P and Evstigneev M 2004 *Phys. Rev. Lett.* **93** 230802
[16] Krylov S Yu, Jinesh K B, Valk H, Dienwiebel M and Frenken J W M 2005 *Phys. Rev.* E **71** 065101
[17] Gnecco E, Bennewitz R, Gyalog T and Meyer E 2001 *J. Phys: Condens. Matter* **13** R619
[18] Riedo E, Gnecco E, Bennewitz R, Meyer E and Brune H 2003 *Phys. Rev. Lett.* **91** 084502
[19] Sang Y, Dube M and Grant M 2001 *Phys. Rev. Lett.* **87** 174301
[20] Fusco C and Fasolino A 2005 *Phys. Rev.* B **71** 045413
[21] Gomer R 1990 *Rep. Prog. Phys.* **53** 917
[22] Brune H 1998 *Surf. Sci. Rep.* **31** 121
[23] Wang S C and Ehrlich G 1997 *Phys. Rev. Lett.* **79** 4234
[24] Krylov S Yu 1999 *Phys. Rev. Lett.* **83** 4602
[25] Dienwiebel M, Pradeep N, Verhoeven G S, Zandbergen H W and Frenken J W M 2005 *Surf. Sci.* **576** 197
[26] Maier S, Sang Yi, Filleter T, Grant M, Bennewitz R, Gnecco E and Meyer E 2005 *Phys. Rev.* B **72** 245418
[27] Socoliuc A, Gnecco E, Maier S, Pfeiffer O, Baratoff A, Bennewitz R and Meyer E 2006 *Science* **313** 207
[28] Krylov S Yu, Dijksman J A, van Loo W A and Frenken J W M 2006 *Phys. Rev. Lett.* **97** 166103
[29] Evstigneev M, Schirmeisen A, Jansen L, Fuchs H and Reimann P 2006 *Phys. Rev. Lett.* **97** 240601
[30] Johnson K and Woodhouse J 1998 *Tribol. Lett.* **5** 155
[31] Reimann P and Evstigneev M 2005 *New J. Phys.* **7** 25
[32] Abel D, Krylov S Yu and Frenken J W M 2007 *Phys. Rev. Lett.* **99** 166102